Finite Size Effects in Antiferromagnetic Highly Strained BiFeO 3 Multiferroic Films

Daniel Sando, Florian Appert, Oliver Paull, Shintaro Yasui, Dimitrios Bessas, Abdeslem Findiki, Cécile Carrétéro, Vincent Garcia, Brahim Dkhil, Agnès Barthelemy, et al.

ADVANCED PHYSICS RESEARCH Open Access
www.advphysicsres.com

Finite Size Effects in Antiferromagnetic Highly Strained $BiFeO_3$ Multiferroic Films

Daniel Sando, Florian Appert, Oliver Paull, Shintaro Yasui, Dimitrios Bessas, Abdeslem Findiki, Cécile Carrétéro, Vincent Garcia, Brahim Dkhil, Agnès Barthelemy, Manuel Bibes, Jean Juraszek,* and Nagarajan Valanoor*

Epitaxially strain-engineered tetragonal (T)-like $BiFeO_3$ (BFO) is a multiferroic material with unique crystallographic and physical properties compared to its bulk rhombohedral parent. While the effect of this structural change on ferroelectric properties is understood, the influence on correlated antiferromagnetic (AFM) properties, especially with reduced film thickness, is less clear. Here, the AFM behavior of T-like BFO films 9–58 nm thick on $LaAlO_3$ (001) substrates fabricated by pulsed laser deposition was studied using conversion electron Mössbauer spectroscopy and X-ray diffraction. The key findings include: i) Ultrathin T-like BFO films (<10 nm) show a decoupling of magnetic and structural transitions, with the polar vector tilted 32 degrees from [001] in 9–13 nm films. ii) Films thinner than 13 nm exhibit no structural transition down to 150 K, with a Néel (T_N) transition at ≈290 K, ≈35 K lower than thicker films. Interestingly, the T_N scaling with thickness suggests realistic scaling exponents considering a critical correlation length for C-type AFM order, rather than G-type. The results show that finite size effects can tailor transition temperatures and modulate AFM wave modes in antiferromagnetic oxides, with implications for AFM spintronics for future information technologies.

1. Introduction

Antiferromagnets (AFMs) are magnetically ordered materials where neighboring spins align in an antiparallel fashion such that the material possesses a zero net magnetic moment. There is an ever-increasing interest in exploiting AFMs as a platform for spintronics and magnonics, since compared to their ferromagnetic (FM) counterparts, they promise higher operation frequencies (up to THz), allowing for faster devices.[1,2] Moreover, the lack of a net magnetic moment in AFMs makes them immune to parasitic magnetic stray fields, offering opportunities for increased miniaturization and robustness compared to FM devices.[1,3] The better scaling and increased packing density of AFM-based spintronics promise faster computing operations with lower energy consumption.[1,2,4]

Some AFMs, by virtue of their spin arrangements, can harbor spin wave modes (magnons) in the absence of an applied magnetic field. One such material is the perovskite $BiFeO_3$ (BFO): an insulating AFM oxide. BFO's magnetic structure is defined by a long-range cycloidal modulation of the Fe spins, which gives rise to well-defined magnon modes.[5] A key feature of BFO is its multiferroic character: antiferromagnetism coexists with ferroelectricity, i.e., the presence of a spontaneous polarization (P) which can be switched by applied electric field.[6] Importantly, in BFO, the magnetic and ferroelectric order parameters are coupled through the lattice; using an electric field

D. Sando
MacDiarmid Institute for Advanced Materials and Nanotechnology
School of Physical and Chemical Sciences
University of Canterbury
Christchurch 8042, New Zealand

E-mail: daniel.sando@canterbury.ac.nz

The ORCID identification number(s) for the author(s) of this article can be found under https://doi.org/10.1002/apxr.202400068

DOI: 10.1002/apxr.202400068

F. Appert, A. Findiki, J. Juraszek
Univ Rouen Normandie
INSA Rouen Normandie
CNRS
Normandie University
GPM UMR 6634, Rouen F-76000, France
E-mail: jean.juraszek@univ-rouen.fr

O. Paull, N. Valanoor
School of Materials Science and Engineering
UNSW Sydney
Sydney 2052, Australia

S. Yasui
Laboratory for Zero-Carbon Energy
Tokyo Institute of Technology
Ookayama, Meguro, Tokyo 152-8550, Japan

D. Bessas
European Synchrotron Radiation Facility (ESRF)
B.P. 220, Grenoble Cedex F-38043, France

to switch the direction of the polarization modifies the magnetic order[7] and induces shifts in the magnon mode energies.[8]

The sensitivity of BFO's crystal structure to epitaxial (thin film) constraint is well established.[9] A large in-plane compressive strain induces the bulk rhombohedral-like (R-like) phase to undergo a phase transition to a tetragonal-like (T-like) structure.[10] This is a metastable phase with a large axial ratio or tetragonality. The formation of this phase is accompanied by a corresponding modification of ferroelectric, magnetic, and electromechanical properties.[11–13] Whereas the cycloidal modulation is destroyed by strain, the antiferromagnetic character is conserved, with some reports showing G-type AFM order, while others suggest C-type.[14] However, spin-lattice coupling effects in T-like BFO remain largely unexplored. T-like BFO undergoes a magnetic transition from AFM to paramagnetic (PM) near room temperature, with the transition being reported between 320 K (Ref.[15]) and 380 K (Ref.[16]). Interestingly, the crystal structure undergoes a series of structural transitions from monoclinic M_C, to monoclinic M_A (with space groups Pm and Cm respectively), and finally to tetragonal upon increasing temperature.[13]

From a ferroelectric polarization and crystal structure perspective, finite size effects have been studied in T-like BFO (Ref.[17, 18]); however, the same cannot be said of their AFM order parameter. A key question is thus: how does the AFM order parameter scale with thickness in T-like BFO? This is important in multiferroic memory devices, where thickness scaling is often the solution to achieve low-energy FE switching. However, if the size reduction adversely affects the AFM order parameter, it would have implications for AFM spintronic devices.[19,20]

From a fundamental perspective, how the AFM character of T-like BFO behaves at ultrafine thicknesses is equally intriguing. For instance, are the two order parameters (P and M) still coupled at the nanoscale? Is there a fundamental size limit driven by thermal effects and/or domain wall energy and the demagnetizing field (akin to FMs) despite that at the unit cell level, the AFM order in T-like BFO is intrinsically compensated? How do the various monoclinic–tetragonal structural transitions[13] couple (if at all) to the AFM order parameter? It is moreover not clear whether cooperative phenomena such as inverse transitions[21,22] and magnetic and ferroelectric topological defects[23,24] can manifest in T-like BFO at reduced size scales.

Studying the scaling of the AFM order parameter – particularly at the required ultrafine thicknesses – is not a trivial task, as one cannot employ the same techniques typically exploited for FM systems. For instance, approaches using traditional magnetometry are often complicated by the possible contributions from secondary magnetic phases, either in the film itself or in the substrate.[6,25,26] Similarly, probing the magnetic behavior using neutron diffraction is challenging, as the limited sample volume leads to prohibitively long counting times.[27] This complication could—in principle—be overcome using samples in superlattice or multilayer geometries,[28] but this would compromise our understanding of how the breaking of symmetry at a free surface can influence scaling. Whilst scanning NV (nitrogen-vacancy center) magnetometry has been exploited to overcome some of these challenges,[29] it is a highly spatially local technique and currently not capable of measurement over wide temperature ranges. By contrast, ^{57}Fe Mössbauer spectrometry is extremely sensitive to the magnetic properties of iron-containing thin materials, directly probing local magnetic hyperfine interactions at the ^{57}Fe nucleus site. Using the conversion electron Mössbauer spectrometry (CEMS) technique, it can be applied to ultra-thin films, yielding detailed information about the magnetic ordering, magnetic moment, and magnetic interactions within the thin film.[30,31]

Here, we show that ultrathin T-like BFO films can show a decoupling of the magnetic and M_C–M_A structural phase transitions. Using temperature-dependent Mössbauer spectroscopy (laboratory and synchrotron-based) and X-ray diffraction (XRD), we show that T-like BFO films grown on (001) $LaAlO_3$ (LAO) thinner than 13 nm are a true tetragonal phase down to 150 K, while the Néel transition remains at ≈290 K. For a thicker film of 58 nm, the Néel transition occurs almost concurrently with the M_C–M_A structural transition, consistent with previous work.[12,16] Intriguingly, although the 9–13 nm films are nominally a tetragonal structural phase, our CEMS results imply that the polar vector is unexpectedly not along [001] but rather tilted away from it by 32°. These results demonstrate that finite size effects can be used to tailor the transition temperature of antiferromagnetic oxides and once again highlight the power of Mössbauer spectrometry for exploring magnetic order under extreme sample conditions.

2. Results and Discussion

Our study focuses on a set of BFO films 9–58 nm in thickness, grown epitaxially on LAO substrates by pulsed laser deposition (*Experimental Section*). The XRD pattern near the $(001)_{pc}$ reflection (**Figure 1a**) shows a clear thickness-dependent trend of the BFO film peak shape and Laue fringes, while the BFO out-of-plane (*c*) lattice parameter (Figure 1b), calculated from the (001–004) peak positions, shows a discontinuity, such that the *c* parameter is larger for film thicknesses below 20 nm. Notably, the value of *c* for the thinnest films is considerably higher than all reported literature values for T-like BFO grown on LAO.[13] Such an observation suggests that a structural phase transition occurs at a thickness between 13–20 nm; later, we confirm this using advanced XRD techniques.

To examine the possibility that the thickness-dependent structural parameters influence the magnetic order, we used conversion electron Mössbauer spectroscopy (CEMS). This technique probes the hyperfine interactions at the ^{57}Fe nucleus and can give important information on the spin ordering in BFO films.[5,31] When taken at various temperatures, CEMS can also yield information about the magnetic transition temperature.[32] Critical for the present study, when applied to fully enriched ^{57}Fe BFO films,

C. Carrétéro, V. Garcia, A. Barthelemy, M. Bibes
Laboratoire Albert Fert
CNRS
Thales
University Paris-Saclay
Palaiseau 91767, France
B. Dkhil
Université Paris-Saclay
CentraleSupélec
CNRS-UMR8580
Laboratoire Structures
Propriétés et Modélisation des Solides
Gif-sur-Yvette 91190, France

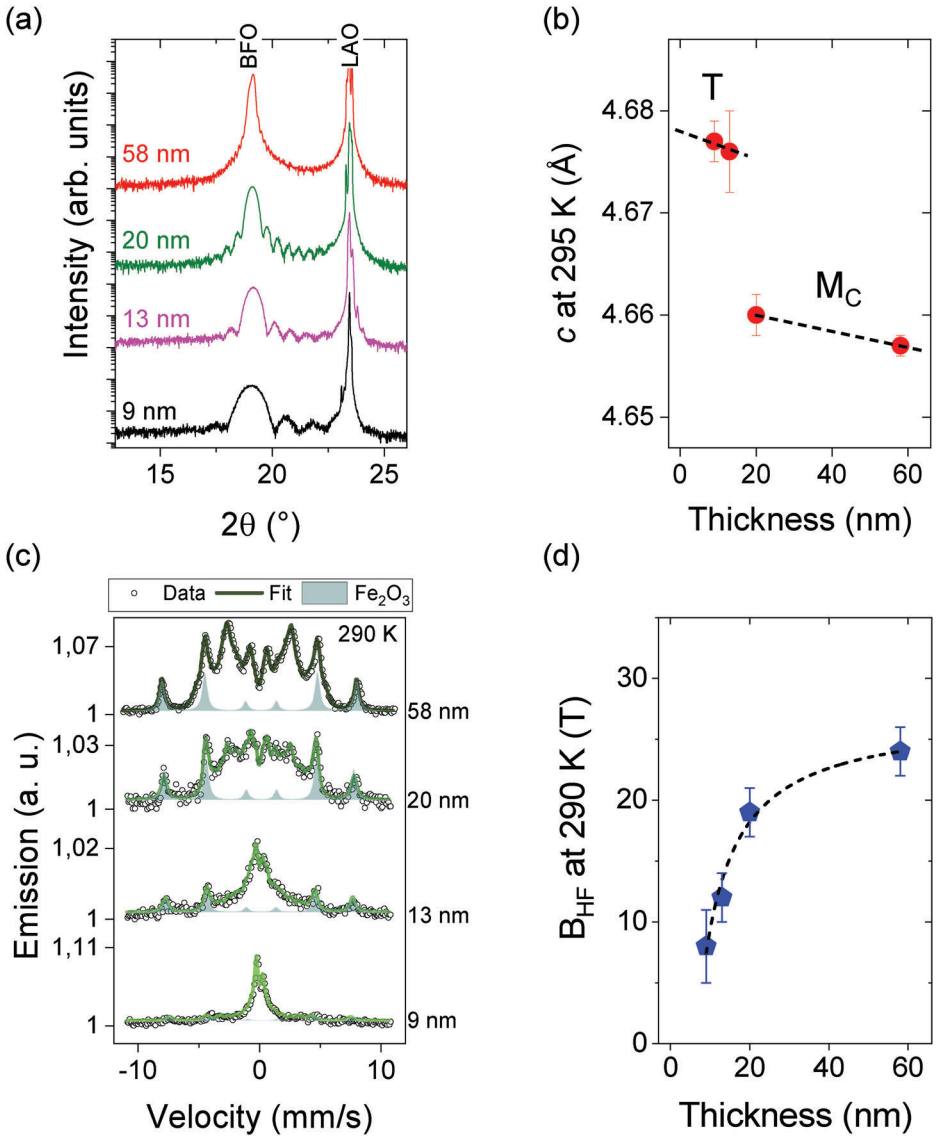

Figure 1. Structural and magnetic properties of thin T-like BFO films. a) X-ray diffraction 2θ-ω scans near the 001 reflections for BFO and LAO. b) BFO out-of-plane *c*-lattice parameter as a function of thickness (determined from the 001–005 BFO peak positions; details in *Experimental Section*), showing a possible structural transition at t ≈20 nm. c) CEMS spectra collected at 290 K, with the data shown as open circles, and fits as solid lines (see text). d) Hyperfine field B_{HF} at 290 K, showing a monotonic decrease in the strength of magnetic interaction. Dashed lines in (b) and (d) are guides to the eye.

CEMS can offer a sufficient signal-to-noise ratio to probe films thinner than 10 nm.[33,34]

The CEMS spectra taken at 290 K, presented in Figure 1c, show that the magnetic order has a strong thickness dependence. We first consider the 58 nm film. The spectrum of this sample exhibits a distinct outer sextet with a hyperfine magnetic field (B_{HF}) of ≈50 T, overlaid by a broader inner magnetic component arising from the overlapping of multiple sets of six-line patterns. Previously it was found in T-like BFO films that such a spectrum arises from Fe^{3+} ions in two separate BFO phases – one T-like phase (broad component) and one R-like phase (sharp sextet with hyperfine field of 49 T).[16] Here, from the fitted hyperfine parameters, and since these films do not contain any detectible relaxed R-like phase (Supporting Information Figure S1), we attribute the outer sextet to Fe^{3+} ions in an impurity phase of α-Fe_2O_3 with a minor spectral area (less than 5%). Although standard structural measurements (not shown) did not detect this phase, it is plausible that CEMS is a more sensitive probe for such minority magnetic phases. The T-like phase component was fitted with a distribution of hyperfine fields, with a mean hyperfine field of $\langle B_{HF} \rangle$ = 24 T. The blue-shaded regions in Figure 1c show the fraction of Fe_2O_3 phase fitted for each film.

Next, we consider the thinnest film of 9 nm. The CEMs spectrum in this case exhibits a two-peak structure (with some much weaker outer peaks, once again related to the Fe_2O_3 phase). The observation of such an extremely narrow set of peaks is consistent with magnetic order at, or very close to, a magnetic transition.[35] Such an observation of the bulk AFM order in a film of this

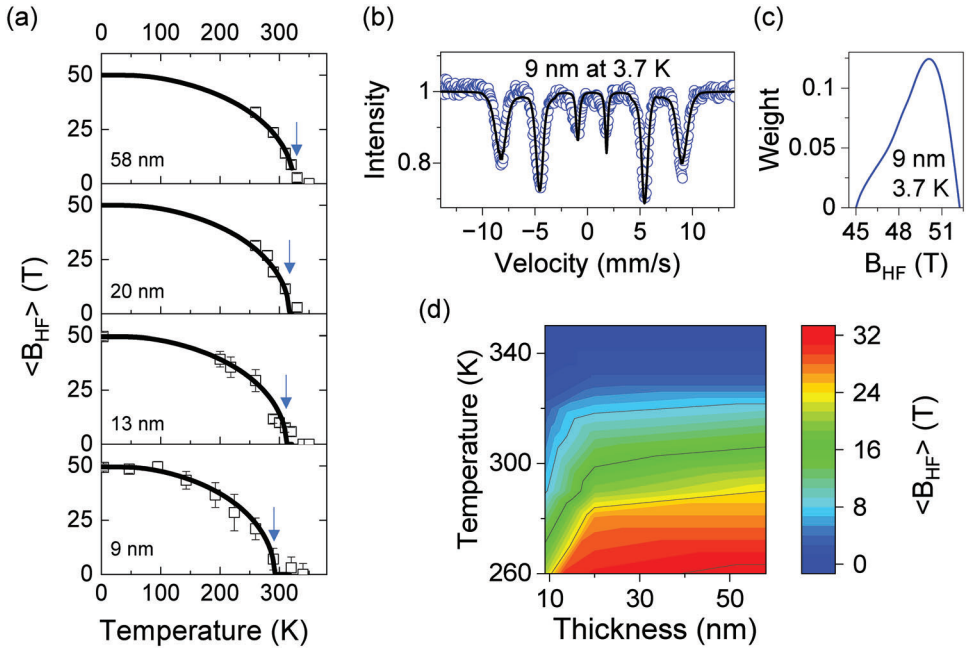

Figure 2. a) Average magnetic hyperfine field $<B_{HF}>$ in T-like $BiFeO_3$ films for various thicknesses obtained using both lab-based (9–58 nm) and synchrotron Mössbauer source (9, 13 nm) measurements. Fits to the data using the Brillouin function are shown as lines. The value of T_N is denoted by the arrow. b) Example of SMS data with data as blue circles, fit as solid lines. c) Example distribution of B_{HF} values used to fit the spectrum in (b). d) Contour plot of $B_{HF}(t, T)$ (from CEMS measurements) showing a clear decrease at low thickness, characteristic of finite size scaling.

thickness is unprecedented, well beyond the means of the classical technique of neutron diffraction.[5,27] Fitting this spectrum with a single sextet (for Fe_2O_3) and distribution of B_{HF} yields an average $<B_{HF}>$ of ≈8 T for the T-BFO phase at room temperature.

Applying the same analysis to the spectra for the other film thicknesses (13 and 20 nm) yields intermediate values of $\langle B_{HF}\rangle$ for the T-BFO phase. When plotted as a function of thickness (Figure 1d), the value of B_{HF} at 290 K is seen to decrease monotonically with decreasing thickness, implying thus that the magnetic order in these films has a dependence on thickness. Interestingly, this transition occurs at a thickness that coincides with the onset of the structural transition as observed in XRD data (Figure 1). This observation provides a *prima facie* case that both the structural and magnetic transitions are intertwined, but we show later that this is not necessarily true.

Having established that the strength of the magnetic interactions in our T-BFO films at 290 K is influenced by thickness, we next consider the antiferromagnetic (Néel) transition temperature T_N: does it also show such a dependence? We explore this in **Figure 2**. To determine T_N in Fe-containing compounds, one can perform CEMS measurements over a wide range of temperatures – including at temperatures above the transition, giving a more accurate determination of T_N.[16,32,36] For this, we used an in-house-developed Peltier thermoelectric cooling-heating setup[37] that allows CEMS measurements between 260 and 350 K (full data in Figures S2 and S3, Supporting Information). Since CEMS measurements at temperatures below 200 K are more challenging, for the 9 and 13 nm films we employed synchrotron Mössbauer source (SMS) experiments at 3–220 K (see Figures S2 and S3, Supporting Information). SMS spectra were measured at the ID18 beamline at the European Synchrotron Radiation Facility (ESRF) (*Experimental Section*) with the sample placed in a He gas exchange cryostat. The full spectra were fitted in the same manner as described in Figure 1c, with a single sextet for the secondary phase, and a distribution of B_{HF} for the T-BFO phase (example shown in Figure 2b,c). Note that some of the B_{HF} distributions show an asymmetry (example distributions for other thicknesses and temperatures in Figure S4, Supporting Information), but there appears not to be a clear trend with either temperature or thickness. The origin of this is currently not known, but it may be that for the thinnest layer, we are probing some proximity effects (the bottom interface with the substrate and the top interface with the air), which modify the electronic and magnetic environment of the Fe site in these regions. Further study would be required to fully explore this scenario. Extracting the mean value of hyperfine field $<B_{HF}>$ for the T-BFO phase at various temperatures yields the trends of the hyperfine field presented for the 4 thicknesses in Figure 2a. Figure 2d is a contour plot (with interpolation) of the same data for temperatures 260–350 K.

For all films, the data show the expected monotonic decrease in hyperfine field strength with temperature.[38] The temperature value at which the B_{HF} value reaches zero is defined as T_N. To determine this value, the data were fitted with a Brillouin function ($J = 5/2$). This approach is analogous to that taken when measuring the intensity of half-order reflections in neutron diffraction as a function of temperature.[14] However, importantly here, by virtue of the ≈100% enrichment in ^{57}Fe, our CEMS measurements can provide unambiguous determination of the AFM order parameter within reasonable measurement timeframes (e.g., a similar measurement by neutron diffraction at 9 nm thickness would require ≈30 days of counting time).

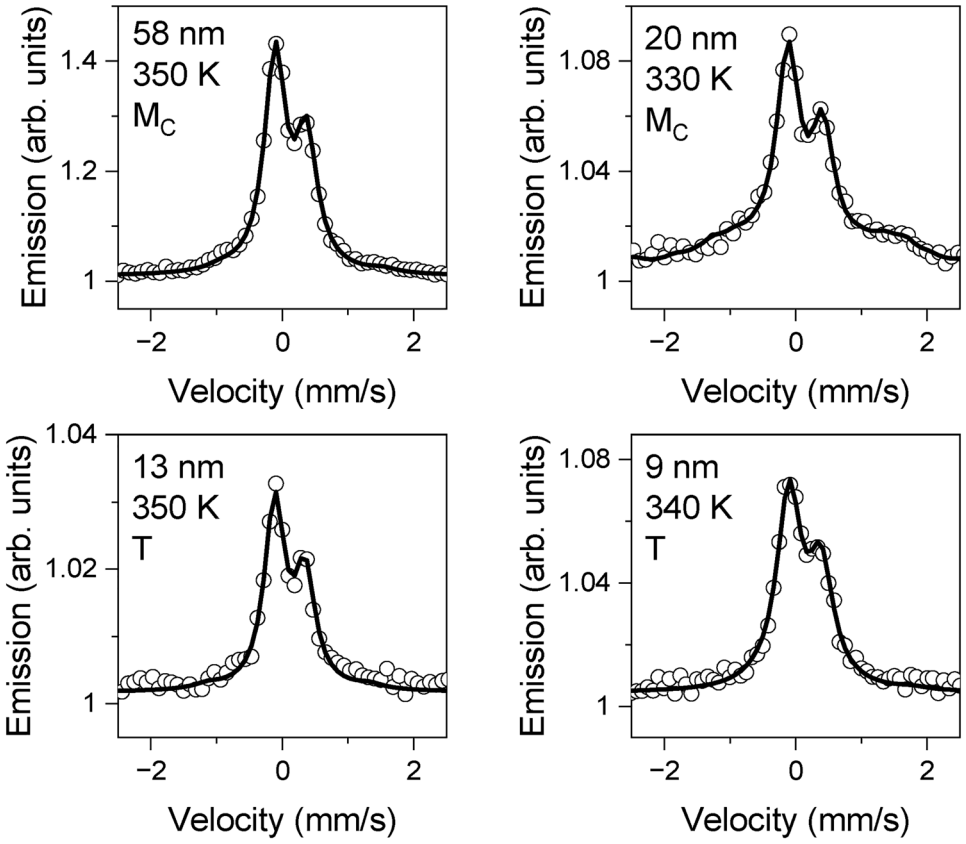

Figure 3. Conversion electron Mössbauer spectroscopy (CEMS) spectra collected at temperatures above the AFM transition. Measured data are open circles, while the fits are shown as solid lines. Note that the relative intensity and spacing of the two peaks, related to the electric field gradient and thus the FE polarization, remains approximately constant for every thickness.

The fittings in Figure 2 reveal that T_N for the thickest film of 58 nm is found to be 324 ± 10 K, in reasonable agreement with the reported value for a thicker 200 nm T-like BFO film by MacDougall *et al.*[14] Interestingly, the T_N found for this T-like BFO film (i.e., without any R-like phase) is considerably lower than the previously reported value of 360 ± 20 K for the T-like component in a 70 nm thick mixed phase R-like/T-like sample grown under the same conditions.[16] From a ferroelectrics perspective, one would expect the opposite behavior–for instance, the critical temperature of a pure tetragonal phase would be higher than the transition for a mixed tetragonal rhombohedral phase.[39] This suggests that the coexistence of R-like and T-like phases can stabilize the AFM order within the T-like fraction to higher transition temperatures, perhaps through a strengthening of the G-AFM order parameter mediated by the R-like/T-like interphase boundaries. This observation requires deeper investigations.

For thinner films, the value of T_N decreases monotonically with thickness, reaching 290 K for the film of 9 nm. To the best of our knowledge, this is the thinnest film of BFO for which T_N has been reported. As we discuss later, the fitting of T_N versus thickness allows us to explore parameters such as the critical exponent and the correlation length.

A further salient feature of the CEMS spectra above the AFM transition is the asymmetry in the paramagnetic quadrupolar doublet. For a single crystal in the case of isotropic recoilless fraction (i.e., in the absence of the Goldanskii-Karyagin effect),[40] the line intensity ratio of the doublet is related to the angle between the main principal axis of the electric field gradient (EFG) at the ^{57}Fe nucleus and the Mössbauer γ-ray direction. In the case of equal intensity of the two lines in the doublet, this angle would be zero – implying an EFG direction along [001]. The CEMS spectra (taken at temperatures above the AFM transition) in a zoomed-in section near 0 mm s^{-1} are presented in **Figure 3**. We find for all films that there is a clear asymmetry in the doublet, with a difference in intensities that cannot be accounted to the less than 5% Fe_2O_3 phase. This means that the direction of the EFG, or in other words, the ferroelectric ***P*** direction, is tilted from the [001] direction by (according to our fits) ≈32 degrees, while (for the 9 and 13 nm films) the shape of the unit cell is tetragonal.

Interestingly, the *magnitude* of the quadrupole splitting is 0.47 mm s^{-1}, ≈7% higher than that observed in bulk BFO and rhombohedral films.[32] Since the magnitude of quadrupole splitting is related to the electric potential at the nucleus (in turn related to the polarization magnitude),[5] then in this simple picture, our results imply that T-like BFO has only 7% higher polarization magnitude than R-like BFO. Such an observation was also made by Bea *et al.*[10] where the giant polarization value of 150 μC cm^{-2} (reported by some authors[41]) was not found. This once again highlights that in highly strained BFO films, various

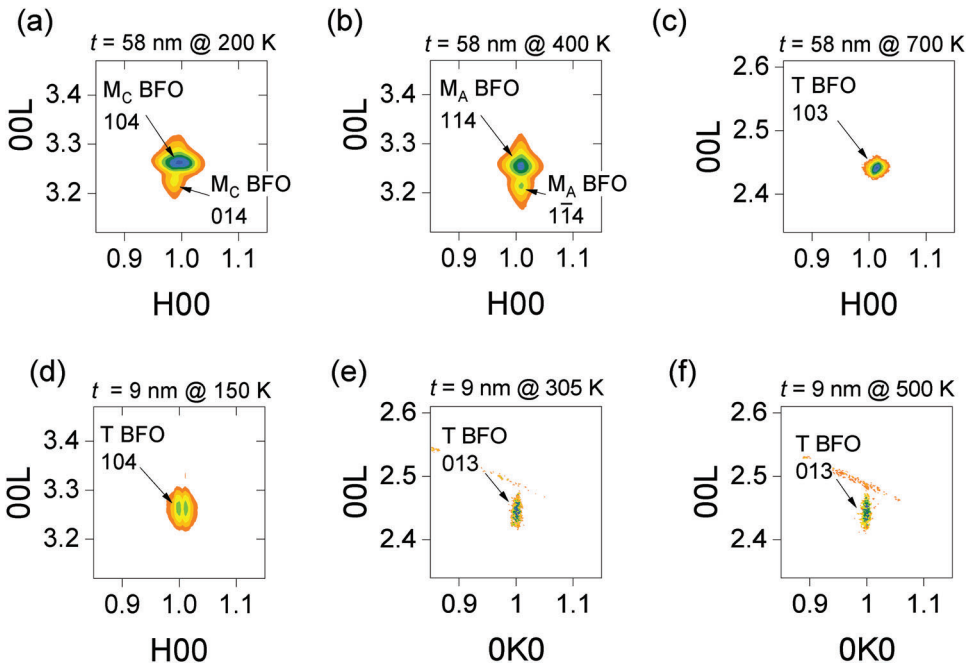

Figure 4. Temperature-dependent XRD reciprocal space mapping. a–c) 58 nm film at 200, 400, and 700 K. The film undergoes a transition from monoclinic M_C to monoclinic M_A, to tetragonal symmetry. d-f) 9 nm film at 150, 305, and 500 K. A single spot is seen at all temperatures, demonstrating that the film is in a tetragonal phase down to 150 K. Note that the horizontal splitting along H00 in d) is due to twinning in the LAO substrate. This splitting is not observed in e) and f) as these RSMs were collected in the 0K0 in-plane direction.

possible structural and polar phases (with differing polarization and structural parameters) can exist.[42,43]

The **P** direction inferred from our measurements—tilted by 32° from [001]—may appear at first glance incompatible with *tetragonal*-like BFO films, but it is instructive to revisit the results of Chen *et al.*, who performed ferroelectric characterization of T-like BFO films using in-plane electrodes.[44] Their study showed a large *in-plane* **P** component – up to 44 μC cm^{-2} along the [100] direction. Combining this value with the out-of-plane magnitude of polarization of 75 μC cm^{-2} measured for some T-like BFO films,[10] yields a **P** vector rotated by ≈30 degrees from [001]. This is consistent with our results from the EFG direction extracted from our CEMS results in Figure 3, at least for the films of 20 and 58 nm which are an M_C phase.

Finally, to conclude this section, we mention that the magnitude of the quadrupole splitting is found to be constant at 0.47 mm s^{-1} for all films (9–58 nm thick), implying that there is no decrease of the **P** magnitude as might be expected for films of thickness approaching the critical thickness. In other words, our CEMS data do not show any evidence of finite size effects on the *ferroelectric* order parameter down to 9 nm thickness.

We next determine if the observed scaling of the Néel temperature is correlated with known structural phase transitions in T-like BFO.[12,13,17,45,46] For this, we collected XRD reciprocal space maps around the (104) or (103) BFO reflections at various temperatures (**Figure 4**). These reflections allow us to distinguish between tetragonal (single peak), monoclinic M_C, or monoclinic M_A structures.[47]

To fully understand the data presented in Figure 4, it is instructive to revisit the structural phase transitions reported thus far for epitaxial BFO. Recall that the T-like BFO phase is only stabilized when grown as an epitaxial thin film under high (≈5%) compressive strain (e.g. on $LaAlO_3$). At room temperature, T-like BFO is a monoclinically distorted M_C phase and possesses a large out-of-plane polarization (but a non-zero in-plane component, as discussed above). T-like BFO undergoes a series of structural phase transitions just above 300 K. Upon increasing temperature, the system traverses a $M_C \rightarrow M_A \rightarrow$ T phase transition series with corresponding transition temperatures ≈400 K and ≈600 K respectively.[13] Following the symmetry of the film, the ferroelectric polarization is (presumed to be) confined to the (010) plane (M_C), to the (110) plane (M_A), and finally to the [001] direction (T) as a function of increasing temperature.

Returning to the data, for the thickest film of 58 nm, the structure was found to be M_C at 200 K (Figure 4a), M_A at 400 K (Figure 4b), and tetragonal at 700 K (Figure 4c), consistent with previous reports on BFO tetragonal-like films of comparable thickness.[17,46] By contrast, the 9 nm thick film shows a single peak at temperatures of 150, 305, and 500 K (Figure 4d,e,f respectively). The presence of a single peak implies a tetragonal structure, meaning that the film maintains the same crystallographic arrangement down to at least 150 K. A similar result was obtained with the 13 nm film (data not shown). These XRD results demonstrate that these T-like BFO films thinner than 20 nm possess – *structurally speaking* – a tetragonal distortion that is maintained down to a very low temperature (as previously observed in Ref.[17]), while the AFM transition remains relatively elevated at 290 K. This demonstrates a clear decoupling of the structural and magnetic transitions.

Further, when compared with the polarization analysis presented in Figure 3, we arrive at an intriguing conclusion: despite crystallizing with a tetragonal structural arrangement, the films

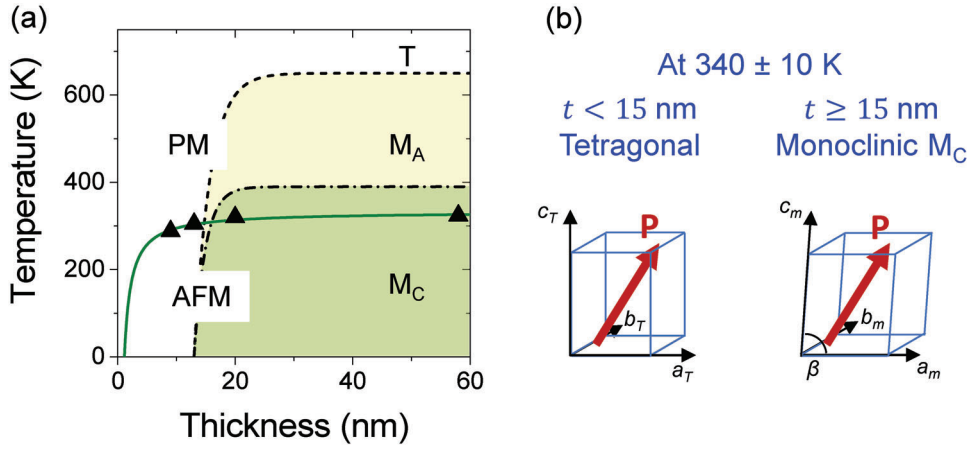

Figure 5. Structure-magnetic order phase diagram for ultrathin T-BFO films. a) For films with thickness < 20 nm, the AFM and M_C-M_A structural phase transitions deviate strongly, demonstrating a decoupling of the transition. b) Despite having a structurally tetragonal unit cell, the films with t < 15 nm have a canted **P** vector, as shown by the red arrow.

of 9 and 13 nm have a **P** direction not strictly locked to the [001] direction (along the *c* axis). Such an observation suggests a situation where the crystallographic structure is tetragonal, but the true symmetry may be reduced. Catalan and Scott have previously inferred a scenario where "the external shape of the unit cell may be tetragonal, (but) the internal degrees of freedom responsible for the polarization might remain monoclinic."[6] Whilst the unambiguous proof of such a concept is challenging, our EFG analysis in Figure 3 hints that this scenario is possible in highly strained BFO. Such observations have been made in other epitaxial thin films, for instance, orthorhombic space group with a tetragonal lattice in $SrTiO_3$ films,[48] or monoclinic distortions in tetragonal phases of $PbTiO_3$ films.[49]

The datasets from Figures 1–4 can be collated to construct the phase diagram presented in **Figure 5**a. We categorize the magnetism as antiferromagnetic (AFM) or paramagnetic (PM), while the structural phase is either tetragonal (T), monoclinic M_C, or monoclinic M_A. The precise value of temperatures of the M_C–M_A and M_A–T transitions for the 20 and 58 nm films were taken from previously reported data[13] to construct the likely transition lines. Note that the phase boundary between AFM and PM is fitted using a finite-scaling law, as discussed next. The phase diagram demonstrates several key points.

First, the AFM–PM Néel transition temperature shows a scaling as expected for critical behavior. Extrapolation of the trend line suggests a critical thickness between 1–2 nm. Since BFO is multiferroic, we compare our results with the FE order parameter as well. Our extrapolated critical thickness is consistent with early works which showed stable ferroelectricity down to at least ≈2 nm in R-like BFO films (grown on $SrTiO_3$ substrates)[50,51] but is much lower than recent reports of the FE transition in BFO with stripe domains.[52] A direct correspondence for the critical thickness of T-like BFO for these thickness ranges is currently unavailable.

The observed scaling of T_N with thickness prompted us to check if we could cast light into critical behavior. Scott *et al.* demonstrated a critical slowing of spin fluctuations in the vicinity of the magnetic transitions for bulk BFO,[53] and we examined if a similar phenomenon can be found (especially for the thinnest cases) since their T_N is decoupled from the structural transition. We attempted to fit the T_N in a critical exponent framework where the Néel temperature has a dependence given by[28,54]

$$1 - \frac{T_N}{T_N(\infty)} = \left(\frac{\xi_0}{t}\right)^{\lambda} \quad (1)$$

where ξ_0 is the correlation length at 0 K, $T_N(\infty)$ is the AFM transition temperature in the bulk limit, $\lambda = \frac{1}{\nu}$ is the shift exponent (inverse of critical exponent), and t is thickness. We neglected the effect of strain, following the arguments of Scott *et al.*[53] Fitting the data yields the line shown in Figure 5a. This fit gives us the product $\xi_0\lambda = 1.185$. Using nominal values of ξ_0 ranging from 0.5 to 1.4 nm, depending on if we consider C-type or G-type AFM respectively, we obtain λ values ranging from 2.37 to 0.85. This yields a critical exponent ν of from 0.42 (when ξ_0 = 0.5 nm) to 1.18 (when ξ_0 = 1.4 nm). Since ν cannot take values larger than 1,[55] this strongly hints that C-type AFM mechanism is dominant for ultrathin T-like BFO. To thoroughly examine this possibility, one would need to grow (and measure) films at much lower thicknesses, which is currently a significant experimental challenge.

A second important feature of Figure 5a is that we see a clear *decoupling* of the structural $M_C \rightarrow M_A$ and AFM → PM transitions, as revealed by the divergence of these phase boundaries at thicknesses below ≈20 nm. Interestingly, in this thickness range, we find that although the crystal structure is nominally tetragonal, the EFG direction is 32° tilted from [001], as highlighted by the schematic unit cells and **P** vector directions shown in Figure 5b. Several groups had initially proposed that the structural and magnetic transitions are coupled,[12,16] but more recently, it was shown that the strength of the coupling between the magnetism and the structural $M_C \rightarrow M_A$ transition is related to the magnitude of the monoclinic β angle. If $\beta \rightarrow 90$, then the coupling strength between the T_N and structural transition becomes zero, and the transitions are essentially "decoupled". A fine-tuning of the coupling strength between these parameters was demonstrated using La doping to modify the monoclinic angle.[56] The confluence of the phase transition temperatures to

300 K at 15 nm in Figure 5 also suggests a multiferroic triple-phase point, very similar to that observed by Jang *et al.*[56] Here, instead of using A-site doping, the triple phase point could be obtained through thickness control.

3. Conclusion

In summary, we have reported a scaling of the antiferromagnetic transition temperature and its coupling to the lattice in T-like BFO films. We find that i) scaling down the film thickness from 58 to 9 nm induces a decrease of ≈40 K in the Néel transition temperature, ii) the unit cell of films below 20 nm has a tetragonal shape (but may possess a canted polar vector), and iii) analysis of the CEMS doublets above the AFM transition finds no finite size effects are detected in the polar order down to 9 nm. In the context of studies on finite size effects in (111)-oriented R-like BFO films,[29] our extrapolated critical thickness for AFM order in T-like BFO is comparable. Our results are important for the design of magnonic, spintronic, and hybrid multiferroic tunneling devices at the nanoscale.

4. Experimental Section

Thin Film Growth and Standard X-ray Diffraction Characterization: BFO films ≈100% enriched in ^{57}Fe with thickness 9–58 nm were grown by pulsed laser deposition on single crystal $LaAlO_3$ (001) substrates.[57,58] A $Bi_{1.15}{}^{57}FeO_3$ ceramic target was ablated with a frequency-tripled Nd:YAG laser at 1 Hz with fluence ≈2 J cm^{-2} while the substrate was kept at 550 °C in an oxygen environment of 6×10^{-3} mbar. After growth, the films were slowly cooled to room temperature in 300 mbar of oxygen. The film thicknesses were determined by X-ray reflectometry. High angle X-ray diffraction (XRD) θ–2θ scans exhibited only 00*l* reflections, indicative of the T-like phase of BFO.[58] The out-of-plane lattice parameter of the BFO layer (Figure 1b) for each film was determined from a linear fit to the positions of the 001–005 Bragg peaks according to $\sin\theta_n = \frac{\lambda}{2d}n$; ($n = 1, 2, 3, 4, 5$), with θ_n the angle at which the *n*th film peak appears, *n* the peak order. The slope of the linear plot is thus given by $slope = \frac{\lambda}{2d}$. Propagation of the standard error from the linear fit yields the error bars presented in Figure 1b.

Conversion Electron Mössbauer Spectrometry: CEMS spectra were collected under normal incidence employing an in-house built He-5% CH_4 gas flow proportional counter in tandem with a 1.5 GBq ^{57}Co source in a Rh matrix operated in constant acceleration mode.[59] Subsequently, the spectra were fit using the histogram method employing the MOSFIT code.[60]

Synchrotron Mössbauer Source: Synchrotron Mössbauer spectroscopy (SMS)[61] data were obtained at the Nuclear Resonance Beamline (ID18) at the European Synchrotron Radiation Facility (ESRF) in Grenoble, France.[62] The (111) pure nuclear Bragg reflection of a $^{57}FeBO_3$ (FBO) single crystal was used to stimulate the nuclear transition of ^{57}Fe in the thin film samples. The FBO crystal was placed on a WissEl velocity transducer operated with a sinusoidal waveform. A standard γ-ray beam (0.5 mm vertically by 1.5 mm horizontally) was directed onto the sample at grazing incidence. Velocity calibration was achieved with a 25 μm thick natural α-Fe foil. Background-free photon flux generated at 14.4 keV was captured using a scintillation detector. The data were fit with the NORMOS program using a distribution of hyperfine field values.

Low and High Temperature XRD Reciprocal Space Mapping: RSMs were obtained for the 9 and 58 nm films at temperatures 150–300 K using a closed cycle cryostat at the 3A beamline at Pohang Accelerator Laboratory, South Korea. High temperature XRD RSMs were collected using a Rigaku Smartlab diffractometer, equipped with Cu $k_{\alpha-1}$ radiation (λ = 1.5406 Å). The splitting of the 103 peak in Figure 4d arises from twinning in the rhombohedral $LaAlO_3$ substrate. This twinning is not observed in Figure 4e,f as the experiment at 305–500 K took place in a different diffractometer and thus the in-plane alignment of the sample was different.

Supporting Information

Supporting Information is available from the Wiley Online Library or from the author.

Acknowledgements

D. S. acknowledges the support of an Australian Nanotechnology Network travel fellowship, and the University of Canterbury Early Career Research Accelerator Fund. This research was partially supported by the Australian Research Council Centre of Excellence in Future Low-Energy Electronics Technologies (Project No. CE170100039) and funded by the Australian Government. D. S. and N. V. acknowledge the support of the Australian Research Council through Discovery Grants. The authors acknowledge the European Synchrotron Radiation Facility for beamtime provision and the helpful discussions with Dr. A. I. Chumakov during data acquisition at the Nuclear Resonance beamline ID18. The authors also thank J.-P. Celse for technical assistance during the preparation of the experiment at ID18. The authors also acknowledge the Pohang Accelerator Laboratory (South Korea) for the provision of experimental time on beamline 3A. S. Y. acknowledges JSPS KAKENHI Grant Numbers 23K23036, 22H01768, and 19H02426, and the Collaborative Research Project of Laboratory for Materials and Structures, Institute of Innovative Research, Tokyo Institute of Technology.

Conflict of Interest

The authors declare no conflict of interest.

Data Availability Statement

The data that support the findings of this study are available from the corresponding author upon reasonable request.

Keywords

antiferromagnet, $BiFeO_3$, finite size, Mössbauer spectroscopy, multiferroic

Received: May 16, 2024
Revised: July 4, 2024
Published online:

[1] J. Han, R. Cheng, L. Liu, H. Ohno, S. Fukami, *Nat. Mater.* **2023**, *22*, 684.
[2] IEEE, International Roadmap for Devices and Systems, "Beyond CMOS and Emerging Materials Integration." Institute of Electrical and Electronics Engineers, **2023** https://doi.org/10.60627/0P45-ZJ55.
[3] V. Baltz, A. Manchon, M. Tsoi, T. Moriyama, T. Ono, Y. Tserkovnyak, *Rev. Mod. Phys.* **2018**, *90*, 15005.
[4] Z. Liu, Z. Feng, H. Yan, X. Wang, X. Zhou, P. Qin, H. Guo, R. Yu, C. Jiang, *Adv. Electron. Mater.* **2019**, *5*, 1900176.
[5] S. R. Burns, O. Paull, J. Juraszek, V. Nagarajan, D. Sando, *Adv. Mater.* **2020**, *32*, 2003711.

[6] G. Catalan, J. F. Scott, *Adv. Mater.* **2009**, *21*, 2463.
[7] A. Haykal, J. Fischer, W. Akhtar, J.-Y. Chauleau, D. Sando, A. Finco, F. Godel, Y. A. Birkhölzer, C. Carrétéro, N. Jaouen, M. Bibes, M. Viret, S. Fusil, V. Jacques, V. Garcia, *Nat. Commun.* **2020**, *11*, 1704.
[8] P. Rovillain, R. De Sousa, Y. Gallais, A. Sacuto, M. Méasson, D. Colson, A. Forget, M. Bibes, A. Barthélémy, M. Cazayous, *Nat. Mater.* **2010**, *9*, 975.
[9] D. Sando, *J. Phys. Cond. Matter* **2022**, *34*, 153001.
[10] H. Béa, B. Dupé, S. Fusil, R. Mattana, E. Jacquet, B. Warot-Fonrose, F. Wilhelm, A. Rogalev, S. Petit, V. Cros, A. Anane, F. Petroff, K. Bouzehouane, G. Geneste, B. Dkhil, S. Lisenkov, I. Ponomareva, L. Bellaiche, M. Bibes, A. Barthélémy, *Phys. Rev. Lett.* **2009**, *102*, 217603.
[11] A. R. Damodaran, C. Liang, Q. He, C.-Y. Peng, L. Chang, Y.-H. Chu, L. W. Martin, *Adv. Mater.* **2011**, *23*, 3170.
[12] K.-T. Ko, M. H. Jung, Q. He, J. H. Lee, C. S. Woo, K. Chu, J. Seidel, B.-G. Jeon, Y. S. Oh, K. H. Kim, W.-I. Liang, H.-J. Chen, Y.-H. Chu, Y. H. Jeong, R. Ramesh, J.-H. Park, C.-H. Yang, *Nat. Commun.* **2011**, *2*, 567.
[13] D. Sando, B. Xu, L. Bellaiche, V. Nagarajan, *Appl. Phys. Rev.* **2016**, *3*, 011106.
[14] G. J. MacDougall, H. M. Christen, W. Siemons, M. D. Biegalski, J. L. Zarestky, S. Liang, E. Dagotto, S. E. Nagler, *Phys. Rev. B* **2012**, *85*, 100406(R).
[15] W. Siemons, G. J. MacDougall, a. a. Aczel, J. L. Zarestky, M. D. Biegalski, S. Liang, E. Dagotto, S. E. Nagler, H. M. Christen, *Appl. Phys. Lett.* **2012**, *101*, 212901.
[16] I. C. Infante, J. Juraszek, S. Fusil, B. Dupé, P. Gemeiner, O. Diéguez, F. Pailloux, S. Jouen, E. Jacquet, G. Geneste, J. Pacaud, J. Íñiguez, L. Bellaiche, A. Barthélémy, B. Dkhil, M. Bibes, *Phys. Rev. Lett.* **2011**, *107*, 237601.
[17] Y. Yang, C. Beekman, W. Siemons, C. M. Schlepütz, N. Senabulya, R. Clarke, H. M. Christen, *APL Mater.* **2016**, *4*, 36106.
[18] S. R. Burns, O. Paull, R. Bulanadi, C. Lau, D. Sando, J. M. Gregg, N. Valanoor, *Phys. Rev. Mater.* **2021**, *5*, 034404.
[19] J. Allibe, S. Fusil, K. Bouzehouane, C. Daumont, D. Sando, E. Jacquet, C. Deranlot, M. Bibes, A. Barthélémy, *Nano Lett.* **2012**, *12*, 1141.
[20] J. Dho, X. Qi, H. Kim, J. L. MacManus-Driscoll, M. G. Blamire, *Adv. Mater.* **2006**, *18*, 1445.
[21] Y. Nahas, S. Prokhorenko, Q. Zhang, V. Govinden, N. Valanoor, L. Bellaiche, *Nat. Commun.* **2020**, *11*, https://doi.org/10.1038/s41467-020-19519-w.
[22] Y. Nahas, S. Prokhorenko, J. Fischer, B. Xu, C. Carrétéro, S. Prosandeev, M. Bibes, S. Fusil, B. Dkhil, V. Garcia, L. Bellaiche, *Nature* **2020**, *577*, 47.
[23] A. Finco, A. Haykal, S. Fusil, P. Kumar, P. Dufour, A. Forget, D. Colson, J. Y. Chauleau, M. Viret, N. Jaouen, V. Garcia, V. Jacques, *Phys. Rev. Lett.* **2022**, *128*, 187201.
[24] V. Govinden, P. Tong, X. Guo, Q. Zhang, S. Mantri, M. M. Seyfouri, S. Prokhorenko, Y. Nahas, Y. Wu, L. Bellaiche, T. Sun, H. Tian, Z. Hong, N. Valanoor, D. Sando, *Nat. Commun.* **2023**, *14*, 4178.
[25] W. Eerenstein, F. D. Morrison, J. Dho, M. G. Blamire, J. F. Scott, N. D. Mathur, *Science* **2005**, *307*, 1203.
[26] H. Béa, M. Bibes, S. Fusil, K. Bouzehouane, E. Jacquet, K. Rode, P. Bencok, A. Barthélémy, *Phys. Rev. B* **2006**, *74*, 020101.
[27] S. R. Burns, D. Sando, B. Xu, B. Dupé, L. Russell, G. Deng, R. Clements, O. H. C. Paull, J. Seidel, L. Bellaiche, N. Valanoor, C. Ulrich, *npj Quantum Mater.* **2019**, *4*, 18.
[28] T. Ambrose, C. L. Chien, *Phys. Rev. Lett.* **1996**, *76*, 1743.
[29] P. Dufour, A. Abdelsamie, J. Fischer, A. Finco, A. Haykal, M. F. Sarott, S. Varotto, C. Carrétéro, S. Collin, F. Godel, N. Jaouen, M. Viret, M. Trassin, K. Bouzehouane, V. Jacques, J. Y. Chauleau, S. Fusil, V. Garcia, *Nano Lett.* **2023**, *23*, 9073.
[30] D. Sando, A. Agbelele, D. Rahmedov, J. Liu, P. Rovillain, C. Toulouse, I. C. Infante, A. P. Pyatakov, S. Fusil, E. Jacquet, C. Carrétéro, C. Deranlot, S. Lisenkov, D. Wang, J.-M. M. Le Breton, M. Cazayous, A. Sacuto, J. Juraszek, A. K. Zvezdin, L. Bellaiche, B. Dkhil, A. Barthélémy, M. Bibes, *Nat. Mater.* **2013**, *12*, 641.
[31] D. Sando, M. Han, V. Govinden, O. Paull, F. Appert, C. Carrétéro, J. Fischer, A. Barthélémy, M. Bibes, V. Garcia, S. Fusil, B. Dkhil, J. Juraszek, Y. Zhu, X. Ma, V. Nagarajan, *Adv. Funct. Mater.* **2020**, *30*, 2000343.
[32] A. Agbelele, D. Sando, I. C. Infante, C. Carrétéro, S. Jouen, J. M. Le Breton, A. Barthélémy, B. Dkhil, M. Bibes, J. Juraszek, *Appl. Phys. Lett.* **2016**, *109*, 042902.
[33] A. Agbelele, *Structure Magnétique de Couches Minces Épitaxiées Du Multiferroique BiFeO3, PhD Thesis*, Université de Rouen, **2015** https://theses.fr/2015ROUES039
[34] T. Kawauchi, K. Fukutani, M. Matsumoto, K. Oda, T. Okano, X. W. Zhang, S. Kishimoto, Y. Yoda, *Phys. Rev. B* **2011**, *84*, 020415.
[35] H. H. Klauss, H. Luetkens, R. Klingeler, C. Hess, F. J. Litterst, M. Kraken, M. M. Korshunov, I. Eremin, S. L. Drechsler, R. Khasanov, A. Amato, J. Hamann-Borrero, N. Leps, A. Kondrat, G. Behr, J. Werner, B. Büchner, *Phys. Rev. Lett.* **2008**, *101*, 077005.
[36] I. C. Infante, S. Lisenkov, B. Dupé, M. Bibes, S. Fusil, E. Jacquet, G. Geneste, S. Petit, A. Courtial, J. Juraszek, L. Bellaiche, A. Barthélémy, B. Dkhil, *Phys. Rev. Lett.* **2010**, *105*, 057601.
[37] F. Appert, *Conception et Réalisation de Détecteurs Dédiés à l'analyse de Couches Minces Par Spectrométrie Mössbauer : Application à l'étude Des Propriétés Magnétiques de Films d'oxydes, Multiferroïques* **2017** University of Rouen, https://theses.hal.science/tel-01778403
[38] M. Przybylski, I. Kaufmann, U. Gradmann, *Phys. Rev. B* **1989**, *40*, 8631.
[39] B. Noheda, *Curr. Opin. Solid State Mater. Sci.* **2002**, *6*, 27.
[40] V. I. Goldanskii, E. F. Makarov, V. V. Khrapov, *Phys. Lett.* **1963**, *3*, 344.
[41] D. Ricinschi, K.-Y. Yun, M. Okuyama, *J. Phys.: Condens. Matter* **2006**, *18*, L97.
[42] O. Diéguez, O. E. González-Vázquez, J. C. Wojdeł, J. Íñiguez, *Phys. Rev. B* **2011**, *83*, 94105.
[43] F. Pailloux, M. Couillard, S. Fusil, F. Bruno, W. Saidi, V. Garcia, C. Carrétéro, E. Jacquet, M. Bibes, A. Barthélémy, G. A. Botton, J. Pacaud, *Phys. Rev. B* **2014**, *89*, 104106.
[44] Z. Chen, X. Zou, W. Ren, L. You, C. Huang, Y. Yang, P. Yang, J. Wang, T. Sritharan, L. Bellaiche, L. Chen, *Phys. Rev. B* **2012**, *86*, 235125.
[45] C. Beekman, W. Siemons, T. Z. Ward, M. Chi, J. Howe, M. D. Biegalski, N. Balke, P. Maksymovych, A. K. Farrar, J. B. Romero, P. Gao, X. Q. Pan, D. A. Tenne, H. M. Christen, *Adv. Mater.* **2013**, *25*, 5561.
[46] H.-J. Liu, H.-J. Chen, W.-I. Liang, C.-W. Liang, H.-Y. Lee, S.-J. Lin, Y.-H. Chu, *J. Appl. Phys.* **2012**, *112*, 052002.
[47] H. M. Christen, J. H. Nam, H. S. Kim, A. J. Hatt, N. A. Spaldin, *Phys. Rev. B* **2011**, *83*, 144107.
[48] F. He, B. O. Wells, S. M. Shapiro, *Phys. Rev. Lett.* **2005**, *94*, 176101.
[49] G. Catalan, A. Janssens, G. Rispens, S. Csiszar, O. Seeck, G. Rijnders, D. H. A. Blank, B. Noheda, *Phys. Rev. Lett.* **2006**, *96*, 127602.
[50] H. Béa, S. Fusil, K. Bouzehouane, M. Bibes, M. Sirena, G. Herranz, E. Jacquet, J.-P. Contour, A. Barthélémy, *Jpn. J. Appl. Phys.* **2006**, *45*, L187.
[51] Y. H. Chu, T. Zhao, M. P. Cruz, Q. Zhan, P. L. Yang, L. W. Martin, M. Huijben, C. H. Yang, F. Zavaliche, H. Zheng, R. Ramesh, *Appl. Phys. Lett.* **2007**, *90*, 252906.
[52] J. J. Steffes, R. A. Ristau, R. Ramesh, B. D. Huey, *Proc. Natl. Acad. Sci. U.S.A.* **2019**, *116*, 2413.
[53] J. F. Scott, M. K. Singh, R. S. Katiyar, *J. Phys. Cond.Matter* **2008**, *20*, 425223.
[54] M. E. Fisher, M. N. Barber Baker, *Phys. Rev. Lett.* **1972**, *28*, 1516.
[55] M. E. Lines, A. M. Glass, *Principles and Applications of Ferroelectrics and Related Materials*, Clarendon Press, Oxford, **1977**.

[56] B.-K. Jang, J. H. Lee, K. Chu, P. Sharma, G.-Y. Kim, K.-T. Ko, K.-E. Kim, Y.-J. Kim, K. Kang, H.-B. Jang, H. Jang, M. H. Jung, K. Song, T. Y. Koo, S.-Y. Choi, J. Seidel, Y. H. Jeong, H. Ohldag, J.-S. Lee, C.-H. Yang, *Nat. Phys.* **2017**, *13*, 189.
[57] D. Sando, A. Agbelele, C. Daumont, D. Rahmedov, W. Ren, I. C. Infante, S. Lisenkov, S. Prosandeev, S. Fusil, E. Jacquet, C. Carretero, S. Petit, M. Cazayous, J. Juraszek, J.-M. Le Breton, L. Bellaiche, B. Dkhil, A. Barthelemy, M. Bibes, *Philosoph.Transact. Royal Soc. A* **2014**, *372*, 20120438.
[58] D. Sando, C. Carrétéro, M. N. Grisolia, A. Barthélémy, V. Nagarajan, M. Bibes, *Adv. Opt. Mater.* **2018**, *6*, 1700836.
[59] J. Juraszek, O. Zivotsky, H. Chiron, C. Vaudolon, J. Teillet, *Rev. Sci. Instrum.* **2009**, *80*, 043905.
[60] J. Teillet, F. Varret, J. Juraszek, MOSFIT program, unpublished n.d.
[61] V. Potapkin, A. I. Chumakov, G. V. Smirnov, J. P. Celse, R. Rüffer, C. McCammon, L. Dubrovinsky, *J. Synchrotron. Radiat.* **2012**, *19*, 559.
[62] R. Rüffer, A. I. Chumakov, *Hyperfine Interact.* **1996**, *97–98*, 589.